



Cite this: RSC Adv., 2025, 15, 38762

## Uptake of $\text{H}^{14}\text{CO}_3^-/\text{^{14}CO}_3^{2-}$ by calcite: impact of ISA and chloride

Rosa Ester Guidone, <sup>\*a</sup> Nils Huber,<sup>a</sup> Frank Heberling, <sup>a</sup> Thomas Sittel, <sup>a</sup> Natalia Palina,<sup>a</sup> Florian Bocchese,<sup>b</sup> Stéphane Brassinnes,<sup>b</sup> Marcus Altmaier<sup>a</sup> and Xavier Gaona <sup>\*a</sup>

The uptake of inorganic  $^{14}\text{C}$  ( $\text{H}^{14}\text{CO}_3^-/\text{^{14}CO}_3^{2-}$ ) by calcite was investigated at  $\text{pH} \approx 8.3$  in the absence and presence of isosaccharinate ( $[\text{ISA}]_{\text{tot}} = 10^{-5}\text{--}0.2 \text{ M}$ ) and chloride ( $[\text{NaCl}]_{\text{tot}} = 10^{-4}\text{--}2.0 \text{ M}$ ). Calcite is representative of the last degradation stage of Portland cement, whereas ISA and chloride are components expected in low- and intermediate level short-lived waste (L/ILW-SL). A moderate  $^{14}\text{C}$  uptake is observed at short contact times, followed by a steady increase of the retention with time resulting in distribution ratios  $\approx 10^3 \text{ L kg}^{-1}$  at  $t = 60$  days. This is explained by fast adsorption, followed by incorporation into the calcite structure through recrystallization phenomena. The minor impact of ISA and chloride on  $^{14}\text{C}$  uptake is possibly related to the formation of Ca-ISA complexes and the alteration of the surface properties of calcite. The modelling of the recrystallization process allows long-term predictions of the  $^{14}\text{C}$  uptake in the context of repositories for L/ILW-SL.

Received 30th July 2025

Accepted 3rd October 2025

DOI: 10.1039/d5ra05547d

[rsc.li/rsc-advances](http://rsc.li/rsc-advances)

### 1 Introduction

The radioactive isotope  $^{14}\text{C}$  ( $t_{1/2} = 5700 \text{ a}$ ) is found in very low concentrations in nature ( $\approx 1 \text{ ppt}$ ), where it is primarily produced in the lower atmosphere layers by  $^{14}\text{N}$  neutron activation triggered by cosmic rays. In nuclear reactors,  $^{14}\text{C}$  is produced by the activation of stable parent isotopes ( $^{14}\text{N}$ ,  $^{13}\text{C}$  and  $^{17}\text{O}$ ) present in *e.g.*, core structural materials, fuel and reactor coolant.<sup>1,2</sup> In the resulting radioactive waste,  $^{14}\text{C}$  can be present as organic compounds (*e.g.*, small carboxylic acids, alcohols, aldehydes or methane) and inorganic carbonate, although the latter is expected to prevail in (near-surface) repositories for low- and intermediate level short-lived waste (L/ILW-SL).<sup>2</sup>

Cementitious materials are extensively used in L/ILW repositories for construction purposes and as a relevant component in the engineered barrier system. Degradation processes determined by the contact with groundwater (as well as surface water in near-surface disposal concepts) will affect the composition of hydrated cement. Degradation is generally discussed as a sequence of four degradation stages (I to IV), although this sequence is also influenced by the cement type and the use of SI such as fly ash or blast furnace slag. Degradation stage I is dominated by the dissolution of Na and K hydroxides and oxides, resulting in  $\text{pH} > 13$ . Under these conditions, portlandite solubility is low and calcium silicate hydrate (C-S-H) phases are defined by high Ca/Si ratio. In the

degradation stage II, the pore water composition is controlled by portlandite solubility, which defines  $\text{pH} \approx 12.5$  and  $[\text{Ca}] \approx 20 \text{ mM}$ . After the complete dissolution of portlandite, the degradation stage III is dominated by the incongruent dissolution of C-S-H, AFm and AFt phases and the decrease of pH from  $\approx 12.5$  to  $\approx 10$ .<sup>3,4</sup> In the last degradation state (IV), C-S-H phases are completely dissolved and the remaining aggregate minerals (*e.g.*, calcite) control the composition and pH (<10) of the pore solution. Calcite is thus expected as one of the main solid phases responsible for the retention of radionuclides in advanced stages of cement degradation. Although other secondary phases (*e.g.*,  $\text{SiO}_2$ , traces of C-S-H phases with low Ca/Si ratio, *etc.*) cannot be excluded at this stage,<sup>5</sup> calcite is expected to control the inorganic carbonate concentration in solution (mainly constitute by  $\text{HCO}_3^-$  aqueous species) and pH with a value of  $\approx 8.3$ .<sup>2,6</sup> Note also that in near-surface disposal concepts, accelerated cement carbonation (and thus calcite formation) needs to be accounted for in specific scenarios. This aspect is of relevance when assessing the retention of  $^{14}\text{CO}_3^{2-}$ , with  $t_{1/2} = 5700 \text{ a}$ .

Calcium carbonate ( $\text{CaCO}_3$ ) exists in several polymorphs (calcite, aragonite and vaterite) or even hydrated forms (hydrated ikaite, monohydrocalcite) depending on the conditions.<sup>7</sup> Calcite is the thermodynamically most stable polymorph of  $\text{CaCO}_3$  at ambient conditions, and it occurs in several geological formations (chalk, limestone, travertine, calcareous sandstone *etc.*).<sup>8</sup> Recrystallization processes can lead to the incorporation of other ions into the calcite structure, as well as to the isotopic exchange with other Ca and C isotopes present in solution. Heberling and co-authors investigated the interlink between recrystallization rates, morphology and particle size of

<sup>a</sup>Karlsruhe Institute of Technology (KIT), Institute for Nuclear Waste Disposal (INE), Hermann-von-Helmholtz-Platz 1, 76344 Eggenstein-Leopoldshafen, Germany. E-mail: rosa.guidone@kit.edu; Xavier.Gaona@kit.edu

<sup>b</sup>ONDRAF/NIRAS, Belgian Agency for Radioactive Waste and Enriched Fissile Materials, Brussels, Belgium



seven calcite samples, from coarse (surface area  $0.2 \text{ m}^2 \text{ g}^{-1}$ ) to fine grained (surface area  $23.8 \text{ m}^2 \text{ g}^{-1}$ ) material following the isotopic exchange with  $^{45}\text{Ca}$ .<sup>9</sup> The authors concluded that calcite recrystallization is an interfacial free energy driven Ostwald-ripening process, in which particle roughness effects dominate over the effect of crystal habitus and particle size. Allard and co-authors<sup>10</sup> investigated the uptake of  $^{14}\text{CO}_3^{2-}$  by natural calcite ( $\text{S/L} = 20 \text{ g L}^{-1}$ ) in artificial granitic pore water ( $\text{pH} = 8.0\text{--}8.2$ ) by means of batch sorption experiments. The authors observed a steady increase of  $^{14}\text{C}$  uptake as function of time with distribution coefficient  $R_d \approx 80 \text{ L kg}^{-1}$  at  $t = 185$  days, and proposed isotopic exchange as main retention mechanism. Boylan and co-workers investigated the retention of  $^{14}\text{CO}_3^{2-}$  following (i) the precipitation of calcite in supersaturation solutions, and (ii) by isotopic exchange with crystalline calcite at  $\text{S/L} = 5, 20$  and  $50 \text{ g L}^{-1}$ .<sup>11</sup> In the experiments conducted in the presence of calcite, the authors observed a minor increase of the uptake of  $^{14}\text{CO}_3^{2-}$  within the monitored time window ( $t = 7\text{--}28$  days) with  $R_d \approx 5 \text{ L kg}^{-1}$ .

Large quantities of cellulose-based materials (*e.g.*, paper, wood, textile, *etc.*) are present in L/ILW-SL. Under the alkaline conditions imposed by cementitious environments, cellulose undergoes degradation resulting in the formation of  $\alpha$ -isosaccharinic acid (ISA) as main degradation product.<sup>12–14</sup> ISA has been shown to form strong complexes with hard Lewis acids such as actinides, lanthanides and some transition metals,<sup>15–19</sup> but forms also weaker complexes with Ca under near-neutral to hyperalkaline pH conditions.<sup>20–22</sup> Although ISA is not expected to interact with  $\text{H}^{14}\text{CO}_3^-/\text{H}^{14}\text{CO}_3^{2-}$ , the impact of this organic ligand on the solubility and surface properties of calcite may affect the retention of this radionuclide. High chloride concentrations (up to  $\approx 4\text{--}5 \text{ M}$ ) are reported for specific waste streams originating from evaporator concentrates in nuclear power plants.<sup>23</sup> These high chloride concentrations can affect the retention of radionuclides in cementitious environments, particularly for anionic radionuclides like  $\text{CO}_3^{2-}$ , for which competition effects may become relevant.

In this context, this work aims at the quantitative description of  $\text{H}^{14}\text{CO}_3^-/\text{H}^{14}\text{CO}_3^{2-}$  uptake by calcite under ambient atmospheric conditions. Moreover, the impact of ISA and chloride on the retention of  $\text{H}^{14}\text{CO}_3^-/\text{H}^{14}\text{CO}_3^{2-}$  is investigated by means of systematic batch sorption experiments on the ternary and quaternary systems calcite- $^{14}\text{C}$ -ISA, calcite-Cl- $^{14}\text{C}$ , and calcite-Cl- $^{14}\text{C}$ -ISA, respectively. Calcite recrystallization and its potential impact on the retention of  $^{14}\text{C}$  is addressed with a dedicated series of inactive batch experiments coupled with modeling approaches previously described in the literature.<sup>9,24</sup>

## 2 Experimental

### 2.1 Chemicals and analytical methods

Milli-Q water (Millipore,  $18.2 \text{ M}\Omega \text{ cm}$ ) was used for the preparation of aqueous solutions. All samples were prepared and equilibrated at  $T = (22 \pm 2)^\circ\text{C}$  under air atmosphere. Active experiments were conducted in dedicated air-gloveboxes.  $\text{CaCO}_3$  was purchased from Sigma-Aldrich (ACS reagent, 99.0%).  $\text{NaCl}$  EMSURE ( $\geq 99.5\%$ ), isosaccharinic acid -1, 4-lactone (ISA<sub>L</sub>) (98.0%), and  $\text{NaOH}$  (and

$\text{HCl}$ ) Titrisol were obtained from Supelco, Biosynth and Merck, respectively. Sorption experiments were performed using  $^{14}\text{CO}_3^{2-}$  as radiotracer. Two  $^{14}\text{CO}_3^{2-}$  ( $t_{1/2} = 5700 \text{ a}$ ) stock solutions were purchased from Eckert & Ziegler Nuclitec GmbH with a purity of  $> 99.9\%$ : (i) a  $^{14}\text{CO}_3^{2-}$  solution in  $\text{Na}_2\text{CO}_3$  as inactive carrier, which was diluted in Milli-Q to obtain the target concentrations of  $[\text{H}^{14}\text{CO}_3^{2-}] = 1.6 \times 10^{-7} \text{ M}$  ( $3.75 \text{ kBq mL}^{-1}$ ) and  $[\text{NaCO}_3] = 4.7 \times 10^{-3} \text{ M}$ ; (ii) a  $^{14}\text{CO}_3^{2-}$  solution in  $0.1 \text{ M NaOH}$  and containing as inactive carrier  $[\text{Na}_2\text{CO}_3] = 2.8 \times 10^{-4} \text{ M}$ , was diluted ( $1:100$ ) in calcite saturated pore solution to achieve  $[\text{H}^{14}\text{CO}_3^{2-}] = 2.4 \times 10^{-7} \text{ M}$  ( $5.58 \text{ kBq mL}^{-1}$ ). Note that at the pH of the experiments ( $\approx 8.3$ ), carbonate is predominantly found as  $\text{HCO}_3^-$  (*ca.* 96%). Keeping this in mind and for the sake of simplicity, the notation  $^{14}\text{C}$  has been used throughout the text instead of referring to  $\text{H}^{14}\text{CO}_3^-/\text{H}^{14}\text{CO}_3^{2-}$ .

The measurement of pH was performed using combination pH-electrodes (Orion Ross, Thermo Scientific) filled with  $3.0 \text{ M KCl}$  freshly calibrated against standard pH buffers ( $\text{pH} = 7\text{--}10$ , Merck).

The measured pH value in aqueous solutions at  $I_m \geq 0.1 \text{ mol kg}^{-1}$ ,  $\text{pH}_{\text{exp}}$ , is an operational apparent value related to the molal proton concentration ( $[\text{H}^+]$ , in  $\text{mol kg}^{-1}$ ) by  $\text{pH}_m = \text{pH}_{\text{exp}} + A_m$ , where  $\text{pH}_m = -\log [\text{H}^+]$  and  $A_m$  is an empirical parameter including the activity coefficient of the proton,  $\gamma(\text{H}^+)$ , and the liquid junction potential of the electrode for a given background electrolyte, ionic strength, temperature and pressure. The values of  $A_m$  for  $\text{NaCl}$  solutions were taken from the literature.<sup>25</sup>

### 2.2 Calcite saturated solution

Calcite saturated solution (CSS) was prepared by equilibrating  $\text{CaCO}_3$  with Milli-Q water ( $\text{S/L} = 1 \text{ g L}^{-1}$ ) under air. The suspension was mixed with a magnetic stirrer (100 rpm) at room temperature for at least 24 hours. Total inorganic carbon content (TIC) of CSS was determined with a Shimadzu (TOC-L) device. To remove possible solid residues in the supernatant solution, the CSS was centrifuged at  $6000 \text{ g}$  for 10 min (Hettich Zentrifugen, EBA 280), or otherwise separated by ultrafiltration using 10 kDa filters (2–3 nm cut-off Nanosep®, Pall Life Sciences). The total calcium concentration in inactive and active samples was determined by inductively coupled plasma-optical emission spectroscopy (ICP-OES, PerkinElmer, Optima8300) and ICP-MS (Inductively Coupled Plasma-Mass Spectrometry, Nexion, 2000P), respectively.

Chloride concentration in CSS was determined by ion chromatography (IC) using a Thermo Fisher (Dionex) ICS-3000 device. This concentration was used as lower limit in the  $^{14}\text{C}$  sorption experiments under varying  $\text{NaCl}$  concentration as described in Section 2.5. The composition of CSS is reported in Table 1, as determined experimentally in this work and calculated using thermodynamic data selected in the ThermoChimie database v.12a.<sup>26</sup>

### 2.3 Characterization of calcite recrystallization: XRD, BET and SEM measurements

Calcite recrystallization was studied with two independent systems, *i.e.*, in the absence and presence of  $2.0 \text{ M NaCl}$ . Batch experiments were prepared by contacting 5 g of calcite with CSS



**Table 1** Composition of the calcite saturated solution (CSS) under air atmosphere used in this work. Uncertainties are reported as two times the standard deviation ( $2\sigma$ ) of mean values. Values in cursive correspond to the CSS composition as calculated using thermodynamic data selected in the ThermoChimie database v.12a.<sup>26</sup>  $C_{\text{tot}}$  indicates the total carbonate concentration expressed as  $[\text{HCO}_3^-] + [\text{CO}_3^{2-}]$

pH	$[\text{Ca}]_{\text{tot}}$ (M)	$C_{\text{tot}}$ (M)	$[\text{Cl}]_{\text{tot}}$ (M)
$(8.3 \pm 0.1)$	$(5.79 \pm 0.27) \times 10^{-4}$	$(1.21 \pm 0.10) \times 10^{-3}$	$(8.40 \pm 0.10) \times 10^{-5}$
8.3	$5.0 \times 10^{-4}$	$1.0 \times 10^{-3}$	

at a solid-to-liquid ratio (S/L) of  $25 \text{ g L}^{-1}$ . Independent batch samples were equilibrated under continuous stirring (100 rpm) for three contact times, *i.e.*,  $t = 2, 14$  and  $82$  days. After the corresponding contact time, solid phase separation was achieved by vacuum filtration through  $0.45 \mu\text{m}$  nylon filters. The resulting wet material was dried in a desiccator for 14 days, and characterized by X-ray powder diffraction (XRD), Brunauer, Emmett and Teller method (BET), and focus ion beam – scanning electron microscopy (FIB-SEM).

XRD measurements were carried out to gain insight on the crystal structure and crystallite size of calcite. Measurements were been performed with a Bruker D8 Advance X-ray powder diffractometer (CuK $\alpha$  radiation,  $\lambda = 1.54184 \text{ \AA}$ ) in the interval  $2\theta = 2\text{--}65^\circ$ , with incremental steps of  $0.012^\circ$  ( $2\theta^\circ$ ) and a total counting time of  $2.0 \text{ s}$  per step.

The specific surface area ( $A_s$ ) of the calcite material after different contact times was determined from gas ( $\text{N}_2$ ) adsorption experiments following the BET method.<sup>27</sup>  $\text{N}_2$ -BET measurements were performed on Quantachrome NOVA 4000e. Samples were dried at  $105^\circ\text{C}$  under vacuum for *ca.* 17 hours before BET measurements.

FIB-SEM images were recorded using a Zeiss FIB-SEM device (CrossBeam 350 KMAT). A secondary electron SE detector (Everhart-Thornley) was used for the characterization of the calcite morphology. FIB-SEM samples were prepared on an Al stab and fixed with a double sided adhesive C-tab.

#### 2.4 Stability of ISA in calcite saturated solution

A stock solution with  $0.1 \text{ M}$  ISA was prepared by dissolving  $0.16 \text{ g}$  of isosaccharinic acid –1,4-lactone ( $\text{ISA}_L$ ) in  $10 \text{ mL}$  of  $0.2 \text{ M}$  NaOH. The solution was equilibrated for 24 hours to trigger the opening of the ISA carbon chain.  $0.5 \text{ mL}$  of  $0.1 \text{ M}$  ISA were added to  $4.5 \text{ mL}$  of CSS to obtain  $[\text{ISA}]_{\text{tot}} = 10 \text{ mM}$ . The excess of NaOH was titrated to  $\text{pH} \approx 8.3$  with  $0.1 \text{ M}$  HCl. The resulting solution was stored under air atmosphere, and characterized at different contacting times ( $t = 2, 7, 14, 30, 60, 160$  days) by  $^1\text{H}$  and  $^{13}\text{C}$  NMR (Nuclear Magnetic Resonance) analysis. NMR analysis was carried out with a Bruker Avance III 400 spectrometer, operating at  $400.18 \text{ MHz}$  for  $^1\text{H}$  and  $100.63 \text{ MHz}$  for  $^{13}\text{C}$ . NMR spectrometer is equipped with a  $5 \text{ mm}$  inverse broadband probe-head furnished with z-oriented magnetic field gradient capability. In each measurement, the magnetic field was stabilized by locking it to the  $^2\text{D}$  signal of the solvent. For the individual samples, 32–64 scans were taken to record  $^1\text{H}$

NMR spectra with the WATERGATE pulse program. The pH was also monitored as a function of time.

#### 2.5 Sorption experiments in the absence and presence of ISA and chloride

Sorption experiments were conducted in  $15 \text{ mL}$  polypropylene vials (Sarstedt) and prepared by contacting fresh calcite with CSS. The suspensions were equilibrated for 1 day before further use. The effect of solid-to-liquid ratio on the uptake was evaluated with independent batch sorption experiments containing  $[\text{C}^{14}\text{C}]_{\text{tot}} = 1.7 \times 10^{-9} \text{ M}$  ( $38.5 \text{ Bq mL}^{-1}$ ) and varying S/L = 5, 25 and  $50 \text{ g L}^{-1}$ . For these samples, the evolution of the activity of  $^{14}\text{C}$  in the aqueous phase was monitored at  $2 \leq t \text{ (days)} \leq 60$ . The uptake of  $^{14}\text{C}$  by calcite was also investigated as a function of the initial  $^{14}\text{C}$  concentration (sorption isotherms), with  $8.6 \times 10^{-11} \text{ M} \leq [\text{C}^{14}\text{C}]_{\text{tot}} \leq 8.6 \times 10^{-9} \text{ M}$ , S/L = 5 and  $25 \text{ g L}^{-1}$  and  $2 \leq t \text{ (days)} \leq 180$ .

The effect of ISA on the retention of  $^{14}\text{C}$  by calcite was investigated as a function of S/L and ISA concentration. In all cases, ISA was added after a pre-equilibration of the suspension containing calcite, CSS and  $^{14}\text{C}$  for two days. A first series of experiments was conducted at  $[\text{C}^{14}\text{C}]_{\text{tot}} = 1.7 \times 10^{-9} \text{ M}$  ( $38.5 \text{ Bq mL}^{-1}$ ),  $[\text{ISA}]_{\text{tot}} = 10^{-2} \text{ M}$ , S/L = 5, 25,  $50 \text{ g L}^{-1}$ , and the activity of  $^{14}\text{C}$  was monitored at  $5 \leq t \text{ (days)} \leq 52$ . A second series of experiments explored the retention of  $^{14}\text{C}$  with increasing ligand concentration, with  $[\text{C}^{14}\text{C}]_{\text{tot}} = 8.6 \times 10^{-9} \text{ M}$  ( $20 \text{ Bq mL}^{-1}$ ), S/L = 5,  $25 \text{ g L}^{-1}$  and  $10^{-4} \text{ M} < [\text{ISA}]_{\text{tot}} < 0.2 \text{ M}$ . The  $^{14}\text{C}$  concentration was monitored at  $12 \leq t \text{ (days)} \leq 289$ . A pH correction was required in samples with high ISA concentration due the alkaline pH ( $\approx 12$ ) of the ISA stock solutions.

The effect of chloride on the retention of  $^{14}\text{C}$  was investigated at NaCl concentrations of  $1 \times 10^{-4}, 3 \times 10^{-3}, 3 \times 10^{-2}, 0.3$  and  $2.0 \text{ M}$ . The suspensions containing calcite, CSS and NaCl were equilibrated for 3 days before the addition of the  $^{14}\text{C}$  tracer. A systematic increase of pH was observed in  $0.3$  and  $2.0 \text{ M}$  NaCl solutions, which required a correction to the target pH value of  $\approx 8.3$ . Sorption experiments were conducted with  $[\text{C}^{14}\text{C}]_{\text{tot}} = 8.6 \times 10^{-9} \text{ M}$  ( $20 \text{ Bq mL}^{-1}$ ) and S/L = 5,  $25 \text{ g L}^{-1}$ .

The combined effect of chloride and ISA on the retention of  $^{14}\text{C}$  was studied with a series of independent batch experiments containing  $[\text{C}^{14}\text{C}]_{\text{tot}} = 8.6 \times 10^{-9} \text{ M}$  ( $20 \text{ Bq mL}^{-1}$ ),  $[\text{ISA}]_{\text{tot}} = 1 \times 10^{-2} \text{ M}$ ,  $10^{-4} \text{ M} < [\text{NaCl}]_{\text{tot}} < 2.0 \text{ M}$ , and S/L = 5,  $25 \text{ g L}^{-1}$ . The suspensions of calcite, CSS and NaCl were equilibrated for 3 days before the addition of  $^{14}\text{C}$ . In a last step, ISA was added after a contact time of 2 days.

The  $^{14}\text{C}$  activity was quantified after phase separation by means of liquid scintillation counting. Phase separation was achieved by ultracentrifugation (90 000 rpm) using an OPTIMA XPN-QC ultracentrifuge and rotor type 90Ti (both Beckman-Coulter). Volumes of *ca.*  $4.2 \text{ mL}$  were transferred into polypropylene tubes (Beckman-Coulter) and heat-sealed afterwards using a tube topper device (Beckman-Coulter, Tube Topper Kit, 60 Hz). LSC measurements were performed using a Tri-Carb 3110 TR. LSC samples were prepared as follows: a variable sample volume ( $0.1\text{--}1 \text{ mL}$ ) was mixed with  $10 \text{ mL}$  of scintillator solution (Hionic-Fluor, PerkinElmer) and  $1.5 \text{ mL}$  of  $2 \text{ M}$  NaOH.



The latter is required to avoid the loss of  $^{14}\text{C}$  through degassing as  $^{14}\text{CO}_2$  due to the acidity of the LSC cocktail. To determine the absolute sample activity (DPM), the measured activity (CPM) was corrected using the appropriate counting efficiency, as described in the SI. The detection limit for  $^{14}\text{C}$  determined by LSC was  $\approx 0.6 \text{ Bq mL}^{-1}$  ( $2.6 \times 10^{-11} \text{ M}$ ).

The retention of  $^{14}\text{C}$  by calcite was evaluated in terms of distribution ratios ( $R_d$ , in  $\text{L kg}^{-1}$ ) as a function of equilibration time, S/L,  $[\text{ISA}]_{\text{tot}}$  and  $[\text{NaCl}]_{\text{tot}}$ .  $R_d$  values are calculated as described in eqn (1):

$$R_d = \frac{[^{14}\text{C}]_{\text{solid}}}{[^{14}\text{C}]_{\text{aq}}} = \frac{A(^{14}\text{C})_{\text{solid}}}{A(^{14}\text{C})_{\text{aq}}} \times \frac{V}{m} = \frac{A(^{14}\text{C})_0 - A(^{14}\text{C})_{\text{aq}}}{A(^{14}\text{C})_{\text{aq}}} \times \frac{V}{m} \quad (1)$$

where  $A(^{14}\text{C})_0$  is the initial  $^{14}\text{C}$  activity,  $V$  is the volume of the solution sample (L) and  $m$  is the mass of calcite (kg). Most  $R_d$  values were quantified by measuring  $A(^{14}\text{C})_0$  and  $A(^{14}\text{C})_{\text{aq}}$  (activity in the aqueous phase, after phase separation). Furthermore, for selected systems,  $R_d$  values were also quantified by measuring  $^{14}\text{C}$  activity in the suspension (aqueous and solid phase) and in the aqueous phase, which reflect the first term of the eqn (1). Both approaches resulted in consistent distribution ratios. Uncertainties in  $R_d$  values were calculated as two times the standard deviation of three sample replicates.

## 2.6 Determination of recrystallization rates

Calcite recrystallization was monitored through the decrease of  $^{14}\text{C}$  activity in solution as a function of the contact time. The fraction of calcite recrystallized was evaluated using the homogeneous and heterogeneous recrystallization models. Both models were initially adapted by<sup>24,28</sup> from the incorporation models described by<sup>29</sup> and.<sup>30</sup> The common assumption in both models is that the ratio of radiotracer ( $^{14}\text{C}$ ) to the carrier element (inactive C) is at any time uniform in the newly formed solid, and equal, to that in solution, see eqn (2). Additionally, as the reaction occurs at the saturation equilibrium of calcite,  $m(\text{C})_{\text{tot}}$  (total aqueous carbonate concentration, in  $\text{mol kg}^{-1}$ ) is assumed to be constant throughout the experiments.

$$\left( \frac{m(^{14}\text{C})}{m(\text{C})_{\text{tot}}} \right)_{\text{solution}} = \left( \frac{n(^{14}\text{C})}{n(\text{C})_{\text{tot}}} \right)_{\text{solid}} \quad (2)$$

where  $m(^{14}\text{C})$  ( $\text{mol kg}^{-1}$ ) and  $n(^{14}\text{C})$  (mol) represent the molality and moles of the radiotracer in solution and the solid phase, respectively.

In the heterogeneous model, the fraction of solid phase recrystallized does not contribute to any further solid-solution equilibration. As a consequence of the heterogeneous model the ratio  $n(^{14}\text{C})/n(\text{C})_{\text{tot}}$  decreases throughout the experiment. Instead, the homogenous model predicts that once a portion of calcite is recrystallized, it is assumed to recrystallize repeatedly over time, maintaining the partial equilibrium between the solution and the calcite that has taken part in the recrystallization process. The moles of recrystallized calcite for the heterogeneous and homogeneous models are calculated according to eqn (3) and (4), respectively:

$$n_{\text{rec}}(t) = \ln \left( \frac{m(^{14}\text{C})_0}{m(^{14}\text{C})(t)} \right) \times W \times m(\text{C})_{\text{tot}} \quad (3)$$

$$n_{\text{rec}}(t) = \left( \frac{m(^{14}\text{C})_0}{m(^{14}\text{C})(t)} - 1 \right) \times W \times m(\text{C})_{\text{tot}} \quad (4)$$

where  $n_{\text{rec}}(t)$  (mol) are the moles of recrystallized calcite at given time  $t$  (s),  $W$  (kg) is the weight of the solution,  $m(^{14}\text{C})_0$  ( $\text{mol kg}^{-1}$ ) is the initial molality of  $^{14}\text{C}$ ,  $m(^{14}\text{C})(t)$  is the molality of the radiotracer at time  $t$  and  $m(\text{C})_{\text{tot}}$  is the total molality of C in the aqueous phase. It is further assumed that calcite with a natural carbon isotopic composition (>99%  $^{12}\text{C}$ ) and  $\text{Ca}^{14}\text{CO}_3$  form an ideal solid solution and that carbon isotope fractionation effects can be neglected during close-to-equilibrium recrystallization.

The recrystallization rates normalized by the surface area  $A_s$  ( $\text{m}^2 \text{ kg}^{-1}$ ) for the experimental time interval  $\Delta t = t_i - t_{i-1}$  (s), are determined as described in eqn (5):

$$r_{\text{rec}} = \frac{(n_{\text{rec}}(t_i) - n_{\text{rec}}(t_{i-1}))}{\Delta t \times A_s} \quad (5)$$

where  $r_{\text{rec}}$  is the recrystallization rate ( $\text{mol (s}^{-1} \text{ m}^2)$ ) and  $n_{\text{rec}}(t_i) - n_{\text{rec}}(t_{i-1})$  (mol) is the difference of the moles of recrystallized calcite in the interval of time  $\Delta t$  (s). The surface area was quantified for analogous inactive systems at the same contact times as in the active experiments (see Section 2.3).

## 3 Results and discussion

### 3.1 Calcite recrystallization

The diffractogram of the original calcite material shown in Fig. 1a is defined by the characteristic diffraction patterns of calcite, with a main feature at  $2\theta^\circ = 29.42^\circ$  ( $d_{(104)} = 3.03 \text{ \AA}$ ). The experimental diffraction peaks fit well with the reference data reported for synthetic calcite (PDF 05-0586). The two planar distances at  $2\theta^\circ = 64.67^\circ$  ( $d_{(300)} = 1.44 \text{ \AA}$ ) and at  $2\theta^\circ = 31.46^\circ$  ( $d_{(006)} = 2.84 \text{ \AA}$ ) confirm rhombohedral crystal configuration ( $R\bar{3}c$ ) with the unit cell parameter:  $a = 4.99 \text{ \AA}$  and  $c = 17.05 \text{ \AA}$ . No further phases are detected. A more comprehensive analysis of the XRD data of calcite, prior to equilibration, is reported in the SI (Fig. S1). The crystalline structure (Fig. 1a) and of the three calcite samples equilibrated at the contacting times,  $t = 2, 14$  and 82 days, is not affected by the recrystallization process.

Fig. 1b shows the diffractograms of calcite samples equilibrated in the presence of 2.0 M NaCl. Calcite is identified as main solid phase, together with traces of NaCl (PDF 05-0628) from adherent NaCl matrix solution. The crystallite size as determined with the Debye–Scherrer method is comparable to the one determined for the NaCl-free system.

The SEM-micrographs and BET specific surface areas of the original calcite material, and samples equilibrated for  $t = 2, 14$  and 82 days are reported in Fig. S2–S4, Fig. S5–S7 (SI) and Table 2, respectively. SEM images of the original calcite material indicate rhombohedral shaped calcite particles, with planar faces and the presence of some surface roughness. SEM pictures reflect also the heterogeneous distribution in the calcite particle



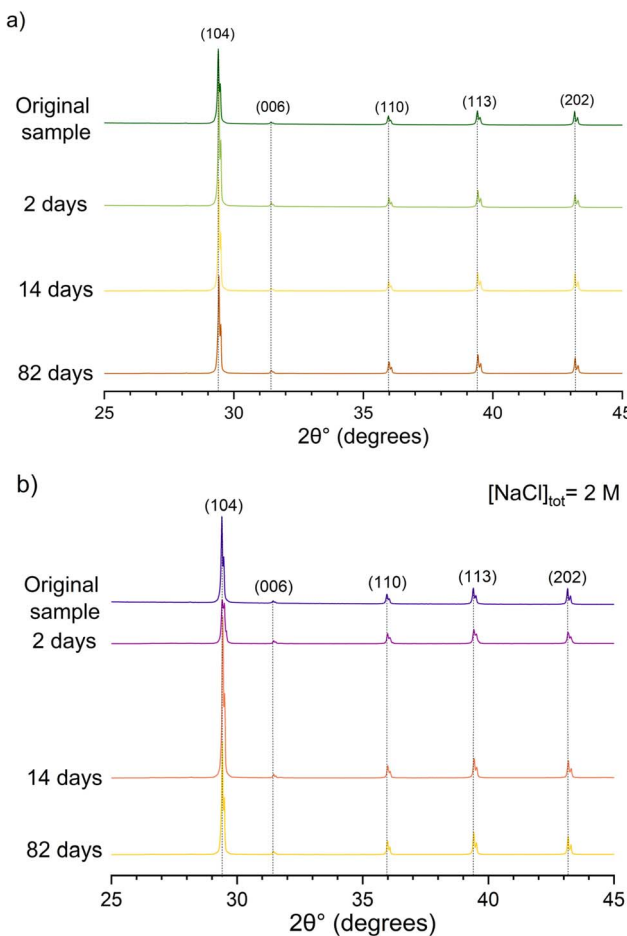


Fig. 1 XRD spectra of calcite samples equilibrated in calcite saturated pore water in the (a) absence and (b) presence of  $[\text{NaCl}]_{\text{tot}} = 2 \text{ M}$  at different contacting times,  $t = 2, 14$  and  $82$  days. The XRD diffractogram of the original calcite material is reported for comparison purposes.

size, with large crystals ( $40\text{--}70 \mu\text{m}$ ) but also abundant smaller particles ( $\leq 500 \text{ nm}$ ). The comparison of the samples at 2 days and 82 days of contacting time, shown in Fig. S2 (SI), qualitatively suggest a decrease of the fraction of smaller particles with increasing contacting time. Sharp interfacial edges were observed for the original calcite material and for the sample equilibrated for 2 days of contacting time. For longer equilibration times ( $t > 2$  days), calcite surfaces become irregular and signs of dissolution processes become more evident (see regions marked in Fig. S3 and S4 in SI).

Table 2 Time evolution of specific surface area ( $A_s$ ) of calcite in the absence and presence of chloride ( $[\text{NaCl}] = 2 \text{ M}$ ), as quantified by BET measurements

Time, (days)	$A_s, (\text{m}^2 \text{ g}^{-1})$	$A_s, (\text{m}^2 \text{ g}^{-1}) [\text{NaCl}] = 2 \text{ M}$
—	$(0.56 \pm 0.05)$	
2	$(0.59 \pm 0.05)$	$(0.40 \pm 0.05)$
14	$(0.47 \pm 0.05)$	$(0.30 \pm 0.05)$
82	$(0.40 \pm 0.05)$	$(0.23 \pm 0.05)$

Both the original calcite material and the sample equilibrated for two days are characterized by a similar surface area ( $A_s \approx 0.6 \text{ m}^2 \text{ g}^{-1}$ ), which is also comparable with the  $A_s$  of calcite sample labelled as “Aged Coarse Cc” in Heberling *et al.*<sup>9</sup> The surface area decreases successively as a function of equilibration time, with  $A_s = 0.47$  and  $0.40 \text{ m}^2 \text{ g}^{-1}$  at  $t = 14$  and  $82$  days of equilibration time, respectively. The observed decreasing trend of  $A_s$  is clearly beyond the uncertainty of the method and can be explained by the increase of the particle size (Fig. S2, SI). This effect is attributed to the Ostwald ripening, particularly affecting to the smaller particles in the calcite material. The SEM micrographs collected for the calcite system in  $2 \text{ M}$  NaCl show also particles with a heterogeneous size distribution, characterized by sharp interfacial edges and partially smooth interfaces (Fig. S5–S7 in SI). BET surface area of calcite in  $2 \text{ M}$  NaCl decreases with time (Table 2), although with slightly lower absolute values compared to chloride-free systems.

### 3.2 $^{14}\text{C}$ retention by calcite

**3.2.1 Uptake of  $^{14}\text{C}$  in the absence of ISA and NaCl.** Fig. 2a and b show the kinetics of the  $^{14}\text{C}$  uptake by calcite at  $S/\text{L} = 5, 25$  and  $50 \text{ g L}^{-1}$ . The uptake increases steadily with time for all three systems, reaching  $R_d \approx 5 \times 10^2 \text{ L kg}^{-1}$  at  $t = 60$  days (Fig. 2a). The slow but steady increase of  $^{14}\text{C}$  uptake with time is attributed to isotopic exchange with  $^{12}\text{C}$  in calcite, triggered by calcite recrystallization. A similar time-dependency of the  $^{14}\text{C}$  uptake by calcite was previously reported by Allard *et al.* (see Fig. 2a), although with overall lower  $R_d$  values.<sup>10</sup> Allard and co-workers performed batch sorption experiments using artificial granitic groundwater with  $\text{pH} = 8.0\text{--}8.2$ ,  $[\text{Ca}]_{\text{tot}} = 4.5 \times 10^{-4} \text{ M}$  and  $[\text{HCO}_3^-]_{\text{tot}} = 2.0 \times 10^{-3} \text{ M}$ , containing as well Na, K, Mg, Cl and  $\text{SO}_4^{2-}$ . Sorption experiments were conducted at  $S/\text{L} = 20 \text{ g L}^{-1}$  with 9 different solid phases, including calcite with particle diameter size of  $63\text{--}90 \mu\text{m}$ . No information was provided on the initial concentration of  $^{14}\text{C}$ . Differences in the absolute  $R_d$  values determined in this work and reported by Allard and co-workers could be eventually caused by differences in particle size of the materials used in both studies, and accordingly in surface area. Moreover, differences in  $R_d$  might be partially influenced by the different pH,  $[\text{Ca}]_{\text{tot}}$  and  $[\text{HCO}_3^-]_{\text{tot}}$  in both experimental datasets. Fig. 2a includes also the experimental results reported by Boylan and co-workers, who investigated the uptake of  $^{14}\text{C}$  by calcite at  $\text{pH} = 8.87$ ,  $[\text{Ca}]_{\text{tot}} = 5 \times 10^{-5} \text{ M}$  and  $C_{\text{tot}} = 2.5 \times 10^{-3} \text{ M}$  within  $t = 7\text{--}30$  days.<sup>11</sup>  $R_d$  values reported by Boylan *et al.*<sup>11</sup> are lower than those reported in this work, but in line with data reported by Allard *et al.*<sup>10</sup> Besides the differences in terms of pH,  $[\text{Ca}]$  and  $C_{\text{tot}}$ , we note that the surface area of the calcite used by Boylan *et al.*<sup>11</sup> ( $0.289 \text{ m}^2 \text{ g}^{-1}$ ) was significantly lower than the calcite material used in this work ( $0.56 \text{ m}^2 \text{ g}^{-1}$ ). Such differences could well explain the discrepancies observed between  $R_d$  values determined in this work and calculated from data reported by Boylan *et al.*<sup>11</sup>

Fig. 2b shows sorption data for the uptake of  $^{14}\text{C}$  by calcite as a function of the  $S/\text{L}$  ratio. The two horizontal solid lines represent the lower ( $0.1 \text{ L kg}^{-1}$ ) and upper ( $10^2 \text{ L kg}^{-1}$ ) limits proposed by Ochs *et al.*<sup>2</sup> for the uptake of  $^{14}\text{C}$  by cement in the



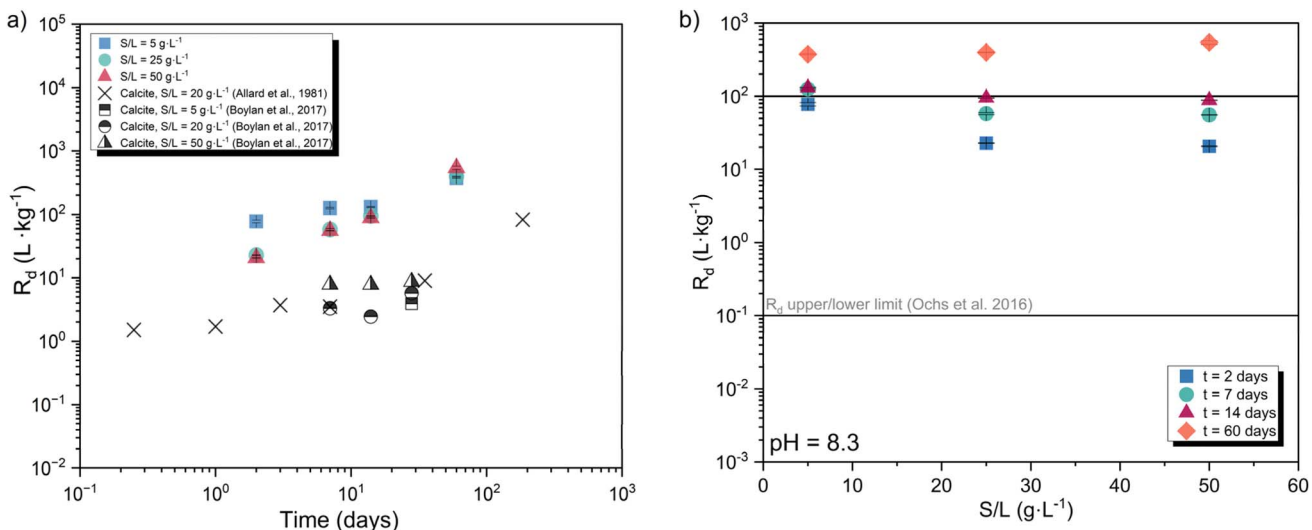


Fig. 2 (a) Sorption kinetics for the uptake of  $^{14}\text{C}$  uptake by calcite for three systems with  $\text{S/L} = 5, 25$  and  $50 \text{ g L}^{-1}$ , obtained in the time frame  $2 \leq t$  (days)  $\leq 60$ . Cross shaped symbols represent the kinetic sorption experiments ( $\text{S/L} = 20 \text{ g L}^{-1}$ ) carried out by Allard et al.<sup>10</sup> and half-filled squares, circles and triangles symbols show the sorption results reported by Boylan et al.<sup>11</sup> (b) Distribution ratios  $R_d$  determined in this work for the uptake of  $^{14}\text{C}$  by calcite as a function of  $\text{S/L}$ . Solid lines represent the upper and lower  $R_d$  limits reported by Ochs et al.<sup>2</sup>

degradation stage IV, *i.e.*, calcite. These upper and lower boundaries are indeed based on the sorption data reported by Allard and co-workers.<sup>10</sup> The figure shows a slight decrease of  $R_d$  values with increasing  $\text{S/L}$  ratio at short contact times, which are expectedly dominated by adsorption processes. Similar observations have been previously described for sorption processes involving other solid phases, *e.g.*, cement or granite.<sup>2,31,32</sup> However, there is no definitive explanation for this observation so far.

Sorption isotherms in Fig. 3 show a linear trend over two orders of magnitude in terms of  $^{14}\text{C}$  aqueous concentration ( $[^{14}\text{C}]_{\text{aq}}$ ). As observed in the sorption kinetics study (see Fig. 2),

an increase of the uptake is observed with time, shifting the corresponding isotherms towards lower aqueous and higher sorbed  $^{14}\text{C}$ .

As described in the literature, calcite recrystallization is a key driving force for the incorporation of  $^{14}\text{C}$  *via* isotopic exchange.<sup>9,33</sup> Heberling and co-authors<sup>9</sup> reported that the recrystallization is a surface free-energy driven process and proposed a direct dependency on particle roughness, particle size and morphology. An increase of roughness (higher surface amorphization) and decrease of particle size contribute to an increase of surface free energy and, consequently, of recrystallization rates.<sup>9</sup> Moreover, it is important to consider that calcite particles minimize their surface free energy during recrystallization, accordingly resulting in a decrease of the recrystallization rate during the reaction, which may affect the rate of  $^{14}\text{C}$  incorporation.<sup>34</sup>

**3.2.2 Modelling and mechanistic understanding of calcite recrystallization.** The fraction of recrystallized and the recrystallization rates for the  $^{14}\text{C}$ -calcite system determined on the basis of the homogeneous and heterogeneous models are shown in Fig. S8 and S9 (SI), respectively. The fraction of recrystallized calcite (%  $\text{Cc}$ ) increases as a function of the contact time (Fig. S8, SI), with greater fractions of recrystallized calcite being estimated by the homogeneous model as a consequence of the model assumptions (see Section 2.6). Fig. 4 shows the experimentally measured  $^{14}\text{C}$  activity as a function of time, compared with model calculations (homogeneous and heterogeneous models) conducted using the recrystallization rates summarized in Table 3. As shown in Table 3, average recrystallization rates quantified with the homogenous model results in  $r_{\text{recr}} = (1.4 \pm 0.2) \cdot 10^{-10} \text{ mol m}^{-2} \text{ s}^{-1}$  and a fraction of recrystallized calcite of  $(3 \pm 0.5)\%$ , which corresponds to  $(100 \pm 10)$  calcite monolayers reacted within 60 days. Less consistent rates are determined from the heterogeneous model, with

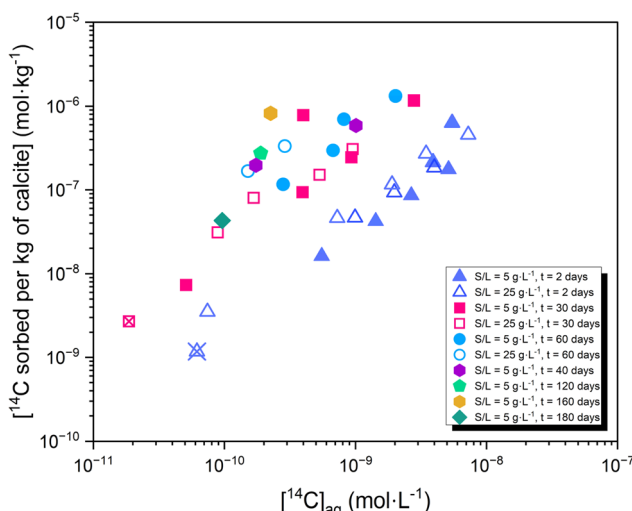


Fig. 3 Sorption isotherms for the uptake of  $^{14}\text{C}$  by calcite at  $\text{S/L} = 5 \text{ g L}^{-1}$  (full symbols) and  $25 \text{ g L}^{-1}$  (empty symbols). Batch sorption experiments were conducted for equilibration times of  $t = 2$ – $180$  days. Crossed symbols are at or below the detection limit.



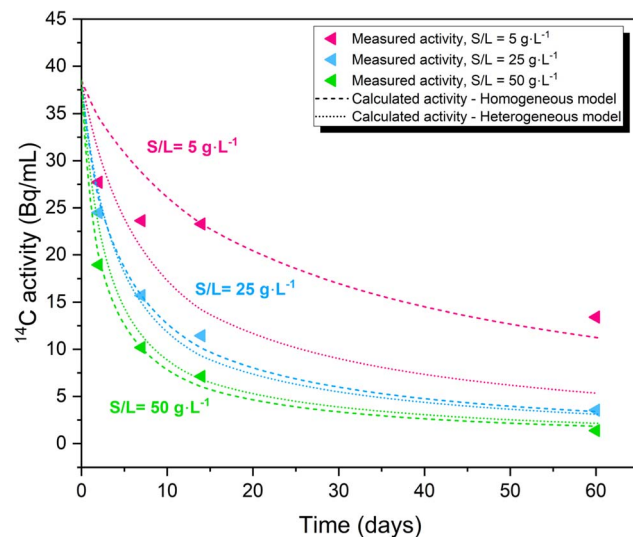


Fig. 4 Comparison of experimental and calculated  $^{14}\text{C}$  activity as a function of time. Calculations conducted with the homogeneous (dashed line) and heterogeneous (dotted line) models, considering the average recrystallization rates summarized in Table 3.

$r_{\text{recr}} = (2 \pm 2) \cdot 10^{-10} \text{ mol m}^{-2} \text{ s}^{-1}$ , corresponding to  $\approx 90$  calcite monolayers. These recrystallization rates are in agreement with the rates reported previously by Heberling and co-workers for a coarse calcite material with surface area of  $\approx 0.2\text{--}0.6 \text{ m}^2 \text{ g}^{-1}$ .

Average recrystallization rates estimated according to the homogenous model allow the prediction of  $R_d$  values for the uptake of  $^{14}\text{C}$  by calcite in the long-term. As shown in Fig. 5 the thermodynamic equilibrium implying the full recrystallization of calcite would result in  $R_d \approx 10^4 \text{ L kg}^{-1}$ , *i.e.* more than one order of magnitude greater than the highest value determined in this work, and more than two orders of magnitude greater than the upper limit reported by Ochs *et al.*<sup>2</sup> Nevertheless, the assumption of thermodynamic equilibrium leading to complete recrystallization of calcite must be considered with some precaution. Calcite recrystallization is understood as a process minimizing the surface-free energy: with the progress of the reaction, the driving force decreases and consequently also the recrystallization rates decrease.<sup>9</sup> Moreover, passivation and the presence of impurity ions may represent a further limit to calcite bulk recrystallization. Hence, the distribution ratio estimated in this work assuming complete equilibration,  $R_d \approx 10^4 \text{ L kg}^{-1}$ , should be considered only as an upper limit for the retention of  $^{14}\text{C}$  by calcite.

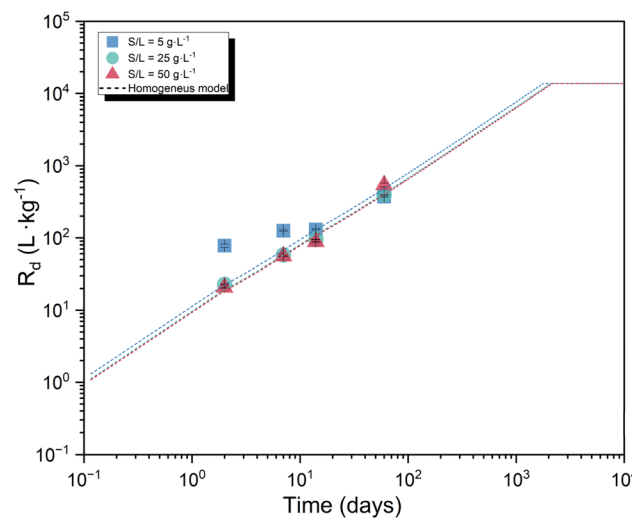


Fig. 5 Time evolution estimated for the uptake of  $^{14}\text{C}$  by calcite according with the homogeneous recrystallization model derived in this work and considering the recrystallization rates reported in Table 3.

### 3.3 Impact of ISA and NaCl on $^{14}\text{C}$ retention

**3.3.1 Uptake of  $^{14}\text{C}$  in the presence of ISA.** The chemical stability of ISA in the weakly alkaline conditions defined by the equilibrium with calcite under air was investigated before initiating the sorption experiments with  $^{14}\text{C}$ . The  $^1\text{H}$  NMR spectra collected (see Fig. S10, SI) shows the typical  $^1\text{H}$  signals of ISA in open chain conformation and are well in agreement with the NMR analyses reported in Brinkmann *et al.* and Jo *et al.*<sup>35,36</sup> No evident changes in the proton signals (new features, shift in peak position or changes in peak shape) have been identified within the investigated time frame,  $t = 2\text{--}160$  days. These results confirm the stability of ISA under the considered boundary conditions, at least for  $t \leq 160$  days.

Fig. 6 shows the distribution ratios determined for the uptake of  $^{14}\text{C}$  by calcite in the presence of ISA ( $10^{-5} \text{ M} \leq [\text{ISA}]_{\text{tot}} \leq 0.2 \text{ M}$ ,  $\text{S/L} = 5 \text{ g L}^{-1}$  and  $t = 12\text{--}289$  days). Similar results were obtained for  $\text{S/L} = 25 \text{ g L}^{-1}$  (see Fig. S11 and S12, in the SI). In general ISA has a relatively minor impact on the uptake of  $^{14}\text{C}$  by calcite. At low ligand concentrations,  $^{14}\text{C}$  retention increases slowly with increasing contacting time, confirming the results obtained for the ISA-free system (see Section 3.2.1). However, with increasing ligand concentration the temporal evolution of the  $R_d$  values decreases, virtually remaining constant for up to

Table 3 Recrystallization rates ( $r_{\text{recr}}$ ) obtained from the fitting of both heterogeneous and homogeneous model for the  $^{14}\text{C}$ -calcite system with  $\text{S/L} = 5, 25$  and  $50 \text{ g L}^{-1}$ . Uncertainties for the recrystallization rates are reported with a 95% of confidence interval, while uncertainties of the average values calculated as two times the standard deviation

$\text{S/L, [g L}^{-1}]$	$r_{\text{recr}} [\text{mol m}^{-2} \text{ s}^{-1}]$ homogeneous model	$r_{\text{recr}} [\text{mol m}^{-2} \text{ s}^{-1}]$ heterogeneous model
5	$(1.61 \pm 1.10) \cdot 10^{-10}$	$(3.48 \pm 2.40) \cdot 10^{-10}$
25	$(1.38 \pm 0.28) \cdot 10^{-10}$	$(1.28 \pm 0.39) \cdot 10^{-10}$
50	$(1.33 \pm 0.38) \cdot 10^{-10}$	$(9.50 \pm 3.15) \cdot 10^{-11}$
Average	$(1.4 \pm 0.2) \cdot 10^{-10}$	$(2 \pm 2) \cdot 10^{-10}$



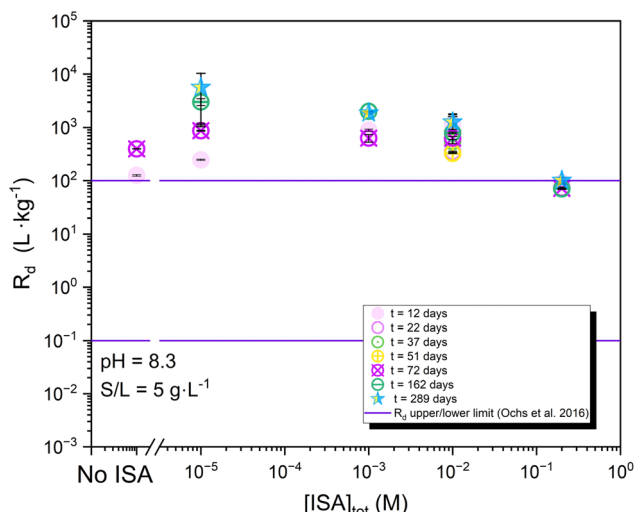


Fig. 6 Distribution ratios ( $R_d$ ) determined for the uptake of  $^{14}\text{C}$  on calcite in presence of ISA ( $[\text{ISA}]_{\text{tot}} = 10^{-5}\text{--}0.2\text{ M}$ ,  $\text{S/L} = 5\text{ g L}^{-1}$ ). Sorption batch experiments were monitored for an equilibration time of  $12 \leq t$  (days)  $\leq 289$ . Solid lines represent the upper and lower  $R_d$  limits reported by Ochs *et al.*<sup>2</sup>

289 days at the highest ISA concentration (0.2 M). This observation possibly reflects that although adsorption of  $^{14}\text{C}$  is not affected by ISA, the presence of this organic ligand may (partially) inhibit calcite recrystallization, subsequently altering the incorporation of  $^{14}\text{C}$  into calcite with time. Indeed, the impact of the adsorption of organic ligands on calcite recrystallization is extensively discussed in the literature for ligands containing different functional groups,<sup>37,38</sup> long-chain carboxylic acids<sup>39</sup> polysaccharides<sup>40</sup> etc. Brune reported also that glucose and sucrose adsorbates delayed the onset and progression of crystallization of amorphous calcium carbonate.<sup>41</sup>

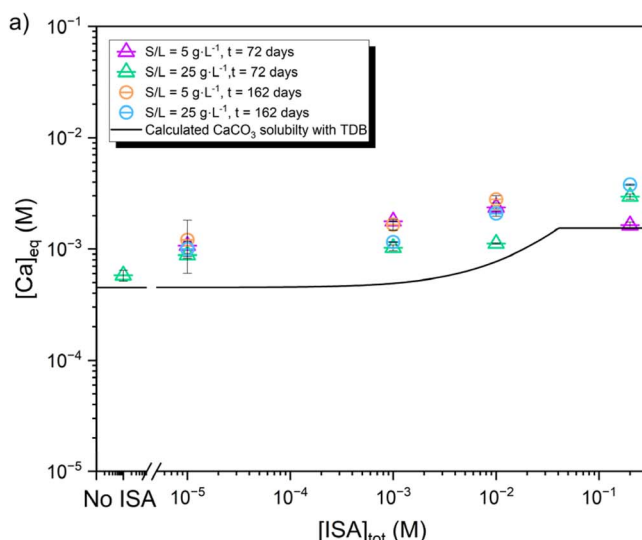


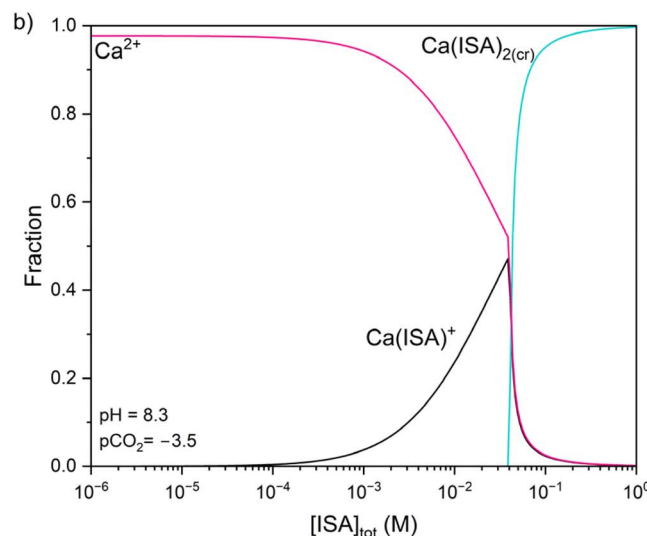
Fig. 7 (a) Experimentally measured Ca concentrations in calcite systems under increasing ISA concentration ( $10^{-5}\text{ M} \leq [\text{ISA}]_{\text{tot}} \leq 0.2\text{ M}$ ) at contact times  $t = 72$  and  $162$  days. Solid line corresponds to the solubility of calcite as calculated with the ThermoChimie database at  $\text{pH} = 8.3$  and  $\text{pCO}_2 = -3.5$ .<sup>26</sup> (b) Ca speciation underlying the solubility curve of calcite shown in Fig. 7a. Calculations conducted with the ThermoChimie database v.12a.<sup>26</sup>

The presence of ISA in solution triggers also the increase of the total Ca concentration in the aqueous phase (Fig. 7a). This increase is consistent with the formation of weak complexes, *i.e.*  $\text{Ca}(\text{ISA})^+$ , although the precipitation of  $\text{Ca}(\text{ISA})_2(\text{cr})$  is also predicted at  $[\text{ISA}]_{\text{tot}} > 0.1\text{ M}$  according to thermodynamic calculations using the ThermoChimie database v.12a (Fig. 7b). The slight apparent decrease of the  $R_d$  values of  $^{14}\text{C}$  observed at  $[\text{ISA}]_{\text{tot}} = 0.2\text{ M}$  could be related to the slight dissolution of calcite, although other effects like the impact of ISA on the surface properties of calcite could also play a role.

### 3.3.2 Uptake of $^{14}\text{C}$ in the presence of NaCl and ISA + NaCl.

Fig. 8 shows the uptake of  $^{14}\text{C}$  in presence of chloride ( $10^{-4}\text{ M} \leq [\text{NaCl}]_{\text{tot}} \leq 2\text{ M}$ ) at contact times of 2 to 60 days, both in the absence (Fig. 8a) and presence (Fig. 8b) of  $[\text{ISA}]_{\text{tot}} = 0.01\text{ M}$ . For both systems,  $R_d$  values determined for the uptake of  $^{14}\text{C}$  in the presence of enhanced chloride concentrations are in line but slightly higher than those determined in chloride-free systems. Most of the calculated  $R_d$  values are found slightly above the upper limit reported by Ochs *et al.*<sup>2</sup> On the other hand, the  $^{14}\text{C}$  uptake in chloride containing systems does not follow the same increasing trend with time observed for chloride-free system (see Section 3.2). This may hint towards the impact of chloride on the surface properties and recrystallization of calcite, as discussed above for calcite systems containing ISA. Note also that Quian and co-workers reported a significant decrease of the crystallization rates of calcite at high chloride concentrations, *i.e.*, 3.5 to 14 wt%,<sup>42</sup> in line with the observations obtained in this work.

The surface electrokinetic properties of calcite are known to be impacted by the presence of  $\text{Na}^+$  and  $\text{Cl}^-$  ions in solution. Based on a series of streaming potential and electrical conductivity measurements, Li and co-workers developed a new approach for the characterization of the electrokinetic properties of calcite in contact with increasing NaCl concentrations (1



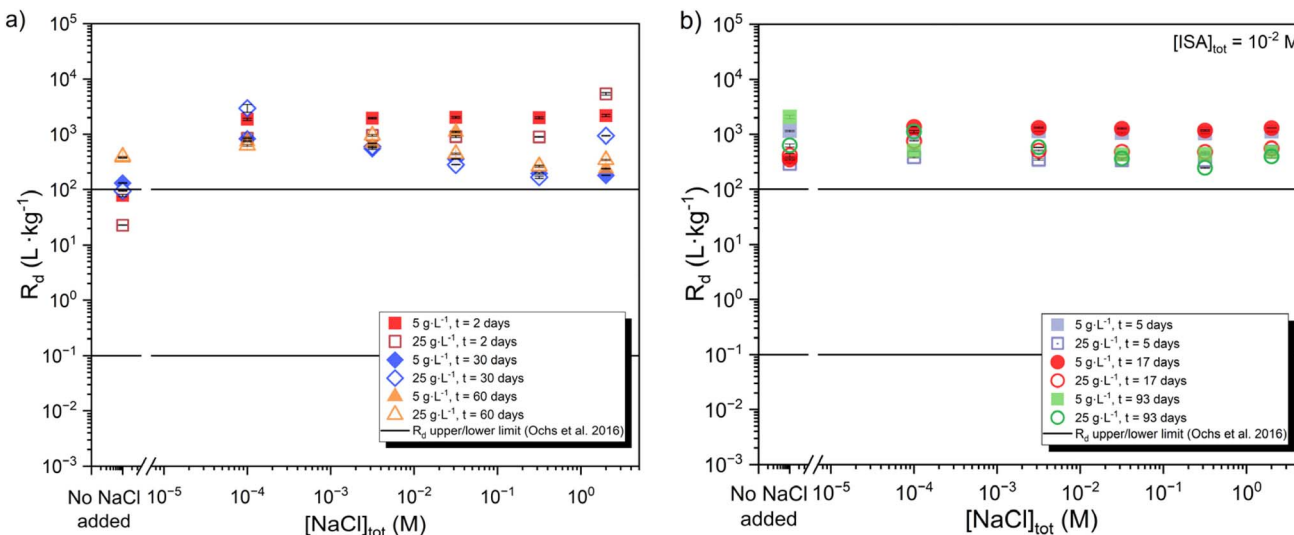


**Fig. 8** Distribution ratios ( $R_d$ ) determined for the uptake of  $^{14}\text{C}$  by calcite at  $\text{pH}_m \approx 8.3$  (a) in the absence and (b) in the presence of ISA ( $[\text{ISA}]_{\text{tot}} = 10^{-2}\text{ M}$ ) as a function of increasing chloride concentration ( $[\text{NaCl}]_{\text{tot}} = 10^{-5}\text{--}2\text{ M}$ ) and  $\text{S/L} = 5$  and  $25\text{ g L}^{-1}$ .  $^{14}\text{C}$  uptake was monitored for contact times of  $t = 2\text{--}60$  and  $5\text{--}93$  days in the absence and presence of ISA, respectively. Solid lines represent the upper and lower  $R_d$  limits reported by Ochs *et al.* for the uptake of  $^{14}\text{C}$  by calcite.<sup>2</sup>

$\times 10^{-3}\text{ M} \leq [\text{NaCl}]_{\text{tot}} \leq 5 \times 10^{-2}\text{ M}$ ) and within the pH range  $5.5 \leq \text{pH} \leq 10.5$ .<sup>43</sup> At  $\text{pH} \approx 8.3$ , the authors reported zeta potentials increasing from  $\approx -40\text{ mV}$  to  $\approx -20\text{ mV}$  at  $[\text{NaCl}] = 1 \times 10^{-3}\text{ to }5 \times 10^{-2}\text{ M}$ , respectively. This trend was also confirmed by Al Mahrouqi and co-workers, who investigated the evolution of the zeta potentials of three natural calcite samples with increasing NaCl concentrations ( $4 \times 10^{-2}\text{ M} < [\text{NaCl}]_{\text{tot}} < 5\text{ M}$ ).<sup>44</sup> In calcite systems containing 2 M NaCl concentrations, the authors reported zeta potentials ranging from  $\approx -6\text{ mV}$  (Portland calcite) to  $\approx +1\text{ mV}$  (Estaijades calcite). Al Mahrouqi and co-workers observed an increase of the Ca concentration in solution with increasing NaCl concentration. This was explained by

a decreased interaction of  $\text{Ca}^{2+}$  ions with the calcite surface due to the increasing occupancy of hydrated  $\text{Na}^+$  ions in the diffuse layer. We note that the recent surface complexation model for calcite–water interface in the presence of NaCl derived by Heberling and co-workers suggest that the outer-sphere sorption of  $^{14}\text{C}$  plays a minor role in the uptake in chloride-rich systems.<sup>45</sup>

In systems containing ISA and chloride, the presence of this organic ligand is expected to further impact the surface properties of calcite, as discussed in Section 3.2.2 for chloride-free systems and reported in the literature for several organic ligands containing  $-\text{COOH}$  and  $-\text{OH}$  functional groups. The

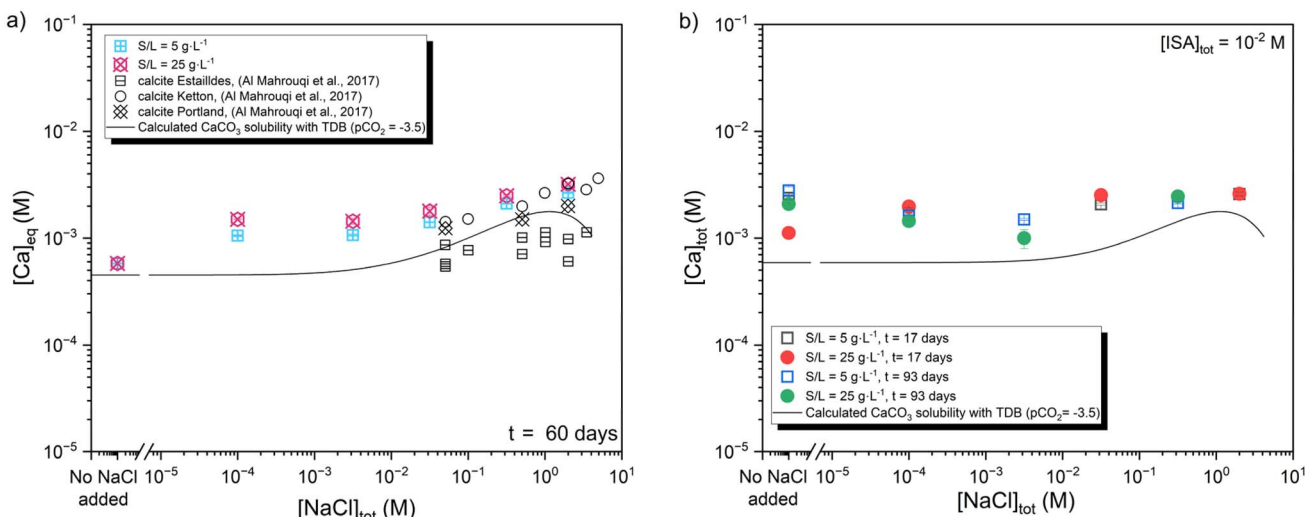


**Fig. 9** Experimentally measured Ca concentrations in calcite systems under increasing NaCl concentrations ( $10^{-4}\text{ M} \leq [\text{NaCl}]_{\text{tot}} \leq 2\text{ M}$ ),  $\text{pH}_m \approx 8.3$ ,  $\text{S/L} = 5$  and  $25\text{ g L}^{-1}$  (a) in the absence of ISA at a contact time of  $t = 60$  days, and (b) in the presence of ISA ( $[\text{ISA}]_{\text{tot}} = 10^{-2}\text{ M}$ ) at contact times of  $t = 17$  and  $93$  days. Solid lines in Figures a and b correspond to the solubility of calcite calculated using the Thermochimie database v.12a and SIT for ionic strength corrections.<sup>26</sup>



presence of NaCl and/or ISA can possibly trigger the dissolution of the most reactive sites/particles prone to dissolution-precipitation processes, but the overall impact quantified in terms of [Ca] evolution as a function of NaCl or [ISA] is relatively minor, as shown in Fig. 7 (ISA system) and Fig. 9 (Cl and ISA + Cl systems).

A slight increase in the total Ca concentration with increasing NaCl concentrations is observed for both  $S/L = 5$  and  $25 \text{ g L}^{-1}$  systems (Fig. 9a). These results are in line with the evolution of the Ca concentration reported by Al Mahrouqi *et al.* for three natural calcite samples under increasing NaCl concentrations (Fig. 9a).<sup>44</sup> From a macroscopic perspective, the increase of Ca concentration is also consistent with the expected increase of calcite solubility, triggered by ion interaction processes in the aqueous phase, as calculated using the ThermoChimie database and SIT for ionic strength corrections (solid line in Fig. 9a). Note however that the fraction of the initially dissolved calcite in 2 M NaCl is very limited, *i.e.*,  $\approx 6\%$  and  $\approx 1.2\%$  at  $S/L = 5$  and  $25 \text{ g L}^{-1}$ , respectively. The presence of  $[\text{ISA}]_{\text{tot}} = 0.01 \text{ M}$  results in a slight increase of Ca concentration compared to ISA-free system and independently of NaCl concentration (Fig. 9b). These observations are in line with the results obtained in the presence of ISA but absence of chloride. The solubility of calcite calculated for these boundary conditions using the ThermoChimie database and SIT for ionic strength corrections explains moderately well the Ca concentrations experimentally measured for this system.

## 4 Conclusions

The uptake of  $^{14}\text{C}$  by calcite was investigated in the presence and absence of ISA and chloride with a comprehensive series of batch sorption experiments at  $\text{pH} \approx 8.3$  under ambient atmosphere (air). Retention was investigated under the variation of  $^{14}\text{C}$ ,  $S/L$  ratio,  $[\text{ISA}]$ ,  $[\text{NaCl}]$  over a timeframe of  $2 \leq t \text{ [days]} \leq 289$ . Calcite recrystallization was evaluated with dedicated series of inactive batch experiments, involving the characterization of calcite as a function of time in terms of crystalline structure, surface morphology and BET surface area.

The crystalline structure of calcite in the absence and presence of chloride ( $[\text{NaCl}] = 2 \text{ M}$ ) remains mostly unaffected, whereas the evolution of the surface morphology highlights surface dissolution and precipitation processes. BET surface area decreases with time, thus supporting the increase of the average particle size through recrystallization phenomena.

Sorption kinetics experiments show a moderate uptake of  $^{14}\text{C}$  at short contact times ( $R_d \approx 20\text{--}70 \text{ L kg}^{-1}$  at  $t = 2 \text{ days}$ ), followed by a systematic increase of the uptake with time resulting in  $R_d \approx 10^3 \text{ L kg}^{-1}$  at  $t = 60 \text{ days}$ . In line with the literature,<sup>2</sup> these results are interpreted in terms of fast surface adsorption followed by the slower incorporation of  $^{14}\text{C}$  into the calcite structure through recrystallization phenomena. Sorption isotherms confirm the linear sorption behavior over  $\approx 10^{-11} \text{ M} \leq [^{14}\text{C}] \leq \approx 10^{-8} \text{ M}$ .

To explore the role of calcite recrystallization in the retention of  $^{14}\text{C}$ , results obtained in the sorption kinetics experiments in combination with BET measurements of the surface area were

interpreted and compared in terms of homogeneous and heterogeneous recrystallization models. The homogeneous model best describes the experimental observations obtained in this work, with average recrystallization rates resulting in  $r_{\text{recr}} = (1.4 \pm 0.2) \cdot 10^{-10} \text{ mol m}^{-2} \text{ s}^{-1}$ . These values are in line with recrystallization rates previously reported in the literature for the uptake of  $^{45}\text{Ca}$  by calcite.<sup>9</sup> The homogeneous recrystallization model was accordingly used for the prediction of  $^{14}\text{C}$  uptake in the long-term. Such predictions assume constant rates and complete calcite recrystallization, and thus may only be considered as upper limits of  $^{14}\text{C}$  sequestration in view of possible secondary processes inhibiting crystallization, *e.g.*, passivation.

ISA has a minor impact on the overall distribution ratios of  $^{14}\text{C}$  determined within  $10^{-5} \text{ M} \leq [\text{ISA}] \leq 0.1 \text{ M}$ . The slight decrease in sorption observed at  $[\text{ISA}] = 0.2 \text{ M}$  is possibly related to the dissolution of calcite through the formation of  $\text{Ca}(\text{ISA})^+$  and  $\text{Ca}(\text{ISA})_2(\text{cr})$ , as evidenced by the quantification of Ca concentration in the aqueous phase and thermodynamic calculations. Remarkably, no increase of the  $^{14}\text{C}$  uptake with time is observed in the presence of ISA, which could be related to the alteration of the calcite recrystallization process triggered by the impact of ISA on the surface properties of calcite.

The presence of NaCl results in a slight increase of the  $^{14}\text{C}$  uptake. Ion interaction processes occurring at high NaCl concentrations result in the slight increase of calcite dissolution, as confirmed by the quantification of Ca concentration in the aqueous phase and thermodynamic calculations. As in the case of ISA, the presence of NaCl minimizes the increase of  $^{14}\text{C}$  uptake with time, eventually due to the alteration of the recrystallization process. Similar distribution coefficients are obtained in sorption experiments containing both ISA and NaCl.

This work provides a quantitative description and improved process understanding for the uptake of  $^{14}\text{C}$  by calcite under conditions relevant for an advanced cement degradation stage in the context of near-surface disposal of L/ILW-SL.

## Author contributions

Rosa Ester Guidone: conceptualization, investigation, methodology, validation, visualization, writing – original draft, writing – review & editing; Nils Huber: investigation, methodology, validation; Frank Heberling: conceptualization, methodology, writing – review & editing; Thomas Sittel: investigation, methodology, validation, writing – review & editing; Natalia Palina: investigation, methodology, validation, writing – review & editing; Florian Bocchese: supervision, conceptualization, writing – review & editing, Stéphane Brassinnes: supervision, conceptualization, writing – review & editing; Marcus Altmaier: supervision, conceptualization, project administrator, writing – review & editing; Xavier Gaona: supervision, resources, conceptualization, methodology, project administrator, writing – review & editing.

## Conflicts of interest

There are no conflicts to declare.



## Data availability

The data supporting this article have been included as part of the SI. Supplementary information is available. See DOI: <https://doi.org/10.1039/d5ra05547d>.

## Acknowledgements

This work was partly funded by ONDRAF/NIRAS (contract number CCHO 2015-0707/00/03). Melanie Böttle, Stephanie Kraft, Stefanie Kuschel, Cornelia Beiser and Tanja Kisely (all KIT-INE) are gratefully acknowledged for the analytical support and characterization of the investigated samples (LSC, ICP-MS/OES, alkaline fusion, TOC/TIC). Julia Podszuweit (KIT-ITC) is kindly acknowledged for the BET measurements of calcite samples.

## References

- 1 M.-S. Yim and F. Caron, *Prog. Nucl. Energy*, 2006, **48**, 2–36.
- 2 M. Ochs, D. Mallants and L. Wang, *Radionuclide and Metal Sorption on Cement and Concrete*, Springer, 2016.
- 3 J. Tits, E. Wieland, M. Bradbury, P. Eckert and A. Schaible, 2002.
- 4 D. Jacques, L. Wang, E. Martens and D. Mallants, *NIRAS-MP5 DATA-LT (NF) Version*, 2008, 1, 2008–2024.
- 5 N. Huber, R. Guidone, X. Gaona, K. Garbev, M. López-García, L. Alcubierre, F. Bocchese, S. Brassinnes, M. Altmaier and H. Geckeis, *Cem. Concr. Res.*, 2025, **197**, 107952.
- 6 J. Tits and E. Wieland, Radionuclide Retention in the Cementitious Near-field of a Repository for Low- and Intermediate-level Waste: Development of the Cement Sorption Database, Nagra, *National Cooperative for the Disposal of Radioactive Waste*, 2023.
- 7 W. A. Deer, R. A. Howie and J. Zussman, *An Introduction to the Rock-Forming Minerals*, Mineralogical Society of Great Britain and Ireland, 2013.
- 8 F. Hammes and W. Verstraete, *Rev. Environ. Sci. Biotechnol.*, 2002, **1**, 3–7.
- 9 F. Heberling, L. Paulig, Z. Nie, D. Schild and N. Finck, *Environ. Sci. Technol.*, 2016, **50**, 11735–11741.
- 10 B. Allard, B. Torstenfelt and K. Andersson, *Sorption Behaviour of 14 C in Groundwater/rock and in Groundwater/concrete Environments*, Programraadet foer Radioaktivt Avfall, 1981.
- 11 A. A. Boylan, D. I. Stewart, J. T. Graham, D. Trivedi and I. T. Burke, *Appl. Geochem.*, 2017, **85**, 137–147.
- 12 M. Glaus, L. Van Loon, S. Achatz, A. Chodura and K. Fischer, *Anal. Chim. Acta*, 1999, **398**, 111–122.
- 13 M. A. Glaus and L. R. Van Loon, *Environ. Sci. Technol.*, 2008, **42**, 2906–2911.
- 14 I. Pavasars, J. Hagberg, H. Borén and B. Allard, *J. Polym. Environ.*, 2003, **11**, 39–47.
- 15 J. Tits, E. Wieland and M. Bradbury, *Appl. Geochem.*, 2005, **20**, 2082–2096.
- 16 X. Gaona, V. Montoya, E. Colàs, M. Grivé and L. Duro, *J. Contam. Hydrol.*, 2008, **102**, 217–227.
- 17 A. Tasi, X. Gaona, D. Fellhauer, M. Böttle, J. Rothe, K. Dardenne, R. Polly, M. Grivé, E. Colàs and J. Bruno, *Appl. Geochem.*, 2018, **98**, 351–366.
- 18 D. Rai and A. Kitamura, *J. Chem. Therm.*, 2017, **114**, 135–143.
- 19 T. Kobayashi, T. Sasaki and A. Kitamura, *J. Chem. Therm.*, 2019, **138**, 151–158.
- 20 K. Vercammen, *Complexation of calcium, thorium and europium by  $\alpha$ -isosaccharinic acid under alkaline conditions*, ETH Zurich, 2000.
- 21 K. Vercammen, M. A. Glaus and L. R. Van Loon, *Acta Chem. Scand.*, 1999, **53**, 241–246.
- 22 W. Hummel, G. Anderegg, L. Rao, I. Puigdoménech and O. Tochiyama, *Chemical Thermodynamics of Compounds and Complexes of U, Np, Pu, Am, Tc, Se, Ni and Zr with Selected Organic Ligands*, Elsevier Amsterdam, 2005.
- 23 L. Wang, E. Martens, D. Jacques, P. D. Canniere, J. Berry and D. Mallants, Review of Sorption Values for the Cementitious Near Field of a Near Surface Radioactive Waste Disposal Facility, *Project Near Surface Disposal of Category a Waste at Dessel (NIROND-TR Report 2008-23E, NIRAS-MP5-03 DATA-LT(NF), V1, Report NIROND-TR Report 2008-23E, NIRAS-MP5-03 DATA-LT(NF))*, Brussels, Belgium, 2009.
- 24 E. Curti, D. Kulik and J. Tits, *Geochim. Cosmochim. Acta*, 2005, **69**, 1721–1737.
- 25 M. Altmaier, V. Metz, V. Neck, R. Müller and T. Fanghänel, *Geochim. Cosmochim. Acta*, 2003, **67**, 3595–3601.
- 26 B. Madé, W. Bower, S. Brassinnes, E. Colàs, L. Duro, P. Blanc, A. Lassin, L. Harvey and J. Begg, *Appl. Geochem.*, 2025, **180**, 106273.
- 27 S. Brunauer, P. H. Emmett and E. Teller, *J. Am. Chem. Soc.*, 1938, **60**, 309–319.
- 28 E. Curti, K. Fujiwara, K. Iijima, J. Tits, C. Cuesta, A. Kitamura, M. Glaus and W. Müller, *Geochim. Cosmochim. Acta*, 2010, **74**, 3553–3570.
- 29 H. A. Doerner and W. M. Hoskins, *J. Am. Chem. Soc.*, 1925, **47**, 662–675.
- 30 W. McIntire, *Geochim. Cosmochim. Acta*, 1963, **27**, 1209–1264.
- 31 E. Wieland, *Sorption Data Base for the Cementitious Near-Field of L/ILW and ILW Repositories for Provisional Safety Analyses for SGT-E2*, Paul Scherrer Institute (PSI), 2014.
- 32 E. Hyeonjin, P. G. Szabo, D. Rehhorn, S. Lee, Y. Jo, M. Altmaier, J. Lee, X. Gaona and J. Yun, *Radiochim. Acta*, 2025, **113**, 181–194.
- 33 M. Prieto, *Rev. Mineral. Geochem.*, 2009, **70**, 47–85.
- 34 A. C. Lasaga, *Kinetic Theory in the Earth Sciences*, Princeton university press, 1998.
- 35 H. Brinkmann, M. Patzschke, P. Kaden, M. Raiwa, A. Rossberg, R. Kloditz, K. Heim, H. Moll and T. Stumpf, *Dalton Trans.*, 2019, **48**, 13440–13457.
- 36 Y. Jo, I. Androniuk, N. Çevirim-Papaioannou, B. de Blochouse, M. Altmaier and X. Gaona, *Cem. Concr. Res.*, 2022, **157**, 106831.
- 37 E. Ataman, M. Andersson, M. Ceccato, N. Bovet and S. Stipp, *J. Phys. Chem. C*, 2016, **120**, 16586–16596.
- 38 O. Qafoku, A. Andersen, W. R. Kew, R. K. Kukkadapu, S. D. Burton, L. Kovarik, Q. Zhao, S. T. Mergelsberg,



T. W. Wietsma and C. T. Resch, *ACS Earth Space Chem.*, 2022, **6**, 1674–1687.

39 M. Ricci, J. J. Segura, B. W. Erickson, G. Fantner, F. Stellacci and K. Voitchovsky, *Langmuir*, 2015, **31**, 7563–7571.

40 M. Yang, S. S. Stipp and J. Harding, *Cryst. Growth Des.*, 2008, **8**, 4066–4074.

41 K. A. Brune, *Master*, University of California, 2016.

42 M. Qian, Y. Zuo, Z. Chen, X. Yin, Y. Liu, W. Yang and Y. Chen, *Crystals*, 2019, **9**, 647.

43 S. Li, P. Leroy, F. Heberling, N. Devau, D. Jougnot and C. Chiaberge, *J. Colloid Interface Sci.*, 2016, **468**, 262–275.

44 D. Al Mahrouqi, J. Vinogradov and M. D. Jackson, *Adv. Colloid Interface Sci.*, 2017, **240**, 60–76.

45 F. Heberling, T. Klačić, P. Raiteri, J. D. Gale, P. J. Eng, J. E. Stubbs, T. Gil-Díaz, T. Begović and J. Lützenkirchen, *Environ. Sci. Technol.*, 2021, **55**, 12403–12413.

